NANO LETTERS

Letter

pubs.acs.org/NanoLett

Scanning Tunneling Spectroscopy on InAs–GaSb Esaki Diode Nanowire Devices during Operation

Olof Persson,[†] James L. Webb,[†] Kimberly A. Dick,[‡,§] Claes Thelander,[‡] Anders Mikkelsen,[†] and Rainer Timm*[,†]

[†]Division of Synchrotron Radiation Research and the Nanometer Structure Consortium (nmC@LU) and [‡]Division of Solid State Physics and the Nanometer Structure Consortium (nmC@LU), Lund University, P.O. Box 118, 221 00, Lund, Sweden

[§]Center for Analysis and Synthesis, Lund University, Box 124, 221 00 Lund, Sweden

Supporting Information

ABSTRACT: Using a scanning tunneling and atomic force microscope combined with in-vacuum atomic hydrogen cleaning we demonstrate stable scanning tunneling spectroscopy (STS) with nanoscale resolution on electrically active nanowire devices in the common lateral configuration. We use this method to map out the surface density of states on both the GaSb and InAs segments of GaSb–InAs Esaki diodes as well as the transition region between the two segments. Generally the surface shows small bandgaps centered around the Fermi level, which is attributed to a thin multielement surface layer, except in the diode transition region where we observe a sudden broadening of the bandgap. By applying a bias to the nanowire we find that the STS spectra shift according to the local nanoscale potential drop inside the wire. Importantly, this shows that we have a nanoscale probe with which we can infer both surface electronic structure and the local potential inside the nanowire and we can connect this information directly to the performance of the imaged device.

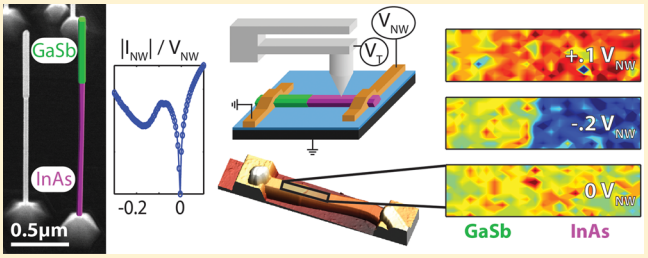

KEYWORDS: *STM, STS, nanowire, InAs, GaSb, Esaki diode*

The III–V semiconductor nanowire (NW) heterostructures have demonstrated strong potential as components in future electronic devices such as LEDs,[1] photovoltaic cells,[2,3] and high-performance/low power transistors.[4] For many such applications, a central property is the ability to tailor complex axial heterostructures along the nanowires without concerns over lattice matching that usually limits heterostructure formation in 2D structures. However, because the nanowires are radially confined to the nanometer scale the structure and chemical composition of the surface play an important role in determining the electrical properties of the nanowires and as a result the device functionality.[5−7] Thus, changes of structural and electronic features in both radial and axial direction are significant even on the nm scale and probes that can address structural and electronic properties along the nanowire surfaces as well as into the nanowires with nanoscale precision are urgently required.

Scanning tunneling microscopy (STM) and scanning tunneling spectroscopy (STS) on nanowires have in recent years been shown to reveal even atomic scale quantitative information on structural and electronic properties both at the surface and inside the nanowires.[8−11] While these measurements have resulted in many important insights, they were all carried out on wires simply deposited on a conducting substrate. What is missing in these studies are means to directly measure on a fully functional nanowire device structure during operation. This is important because the structure (especially at the surface) of the nanowire might change considerably during device fabrication, and physical changes in the structure of the device at the nanoscale may be introduced during operation. Furthermore, it is essential to correlate the performance of a single nanowire device with its specific surface properties. Here we address these issues taking STM/STS on nanowire surfaces a major step further by investigating the behavior of a nanowire device during operation (in situ).

There are two major hurdles to overcome to achieve stable scanning conditions for STM on III–V nanowire devices. First, a functioning device has to be fabricated on an insulating substrate for the current to run through the nanowire. However, this prevents STM scanning off the nanowire and its metal contact electrodes as the tip will crash into the nonconducting substrate surface. Second, the nanowire surfaces are oxidized and possibly with various organic molecules or water adsorbed, making STM/STS highly unstable. To solve the first issue we use a dual mode STM and atomic force microscope (AFM). We can then scan on the complete device and substrate in AFM mode and only run in STM mode when we are positioned on the nanowire or contact surfaces. This requires a careful strategy for performance of the measurements

Received: December 12, 2014
Revised: April 24, 2015
Published: April 30, 2015

DOI: 10.1021/acs.nanolett.5b00898
Nano Lett. 2015, 15, 3684–3691

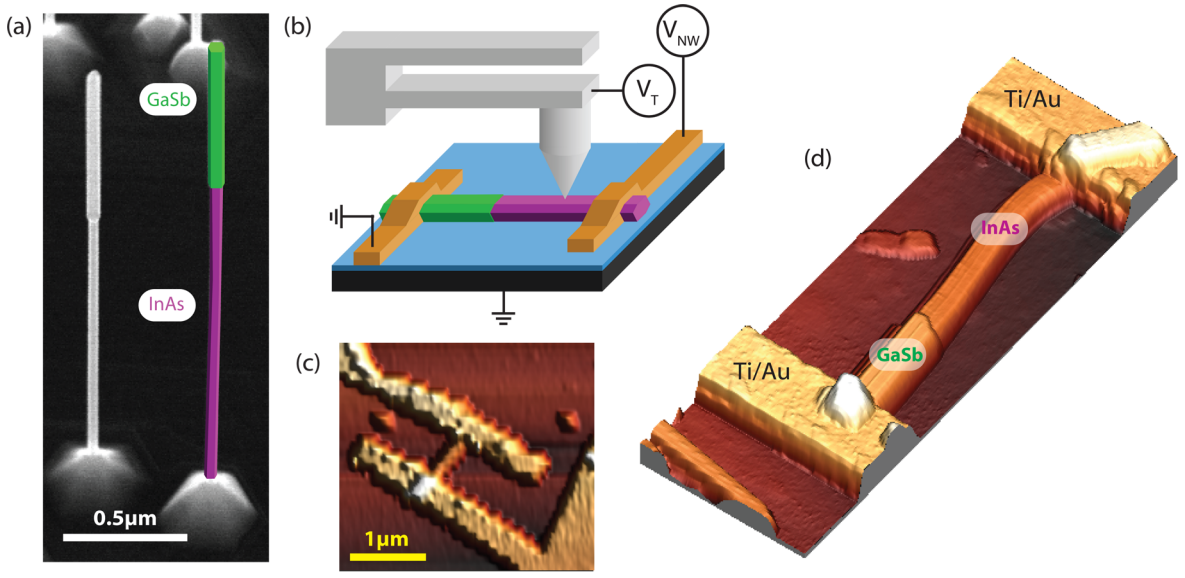

Figure 1. (a) SEM image of the InAs−GaSb nanowires before device fabrication. The thicker top section (50 nm diameter, green) consists of GaSb and the thinner (35 nm, magenta) of InAs. (b) Schematic representation showing the nanowire device and the combined AFM/STM not to scale. The Esaki diode nanowire is contacted with Ti/Au contacts that can be biased externally, V_{NW}, while performing STM on the nanowire. The tip potential is denoted V_T. In this work, the Ti/Au contact to the InAs part is biased while the GaSb contact is grounded. The nanowire device is insulated from the grounded Si substrate (black) by a 200 nm thick SiO_2 layer (blue). (c) The 3D rendering of a 3.5 × 3 μm^2 AFM image showing an overview of a device with the nanowire in the middle with a contact at each end. (d) A higher-resolution AFM image showing the two contacts and the nanowire with the thicker GaSb part (bottom left) clearly distinguishable from the thinner InAs part (top right).

but is nonetheless possible as we show in the present study. The second challenge is addressed here by annealing the sample while exposing to atomic hydrogen from a thermal cracker, which both reduces the amount of the oxide formed on the surface of the nanowires and removes many other volatile contaminants that can interfere with the STM tip. By choosing the right conditions we can remove the surface contaminants sufficiently to allow stable STM/STS while maintaining full device performance, even for complicated nanowire heterostructures with several different III−V compounds.

In this paper, we study InAs−GaSb tunneling (Esaki) diode nanowires exhibiting a characteristic negative differential resistance region. These nanowires are highly promising for applications such as tunnel field-effect transistors and tunneling diodes.[12,13] Here the characteristic negative differential resistance region can be used to monitor that the device is still intact and performing well at all stages of the experiment. Furthermore, the sharp axial heterojunction between the two materials with significantly different band alignment is highly suitable for validating our novel technique where STM/STS measurements can be performed along a biased heterostructure nanowire.

The InAs−GaSb Esaki diode nanowires were grown by low pressure metal−organic vapor phase epitaxy (MOVPE), using hydrogen as carrier gas and size-selected gold aerosol particles with nominal diameter of 30 nm as seeding particles, on InAs (111)B substrates. The InAs section of the nanowire was grown at 450 °C for 13 min using trimethylindium. Tetraethyltin was added after 4 min of growth to n-dope the InAs and switched off 1 min before the end of the InAs growth due to memory effects in the growth chamber. The GaSb section was grown at 500 °C for 20 min using trimethylgallium and trimethylantimony, and diethylzinc was used to p-dope the GaSb. Further details of the growth can be found in ref 14. Figure 1a shows an SEM image of the nanowires still on the growth substrate, illustrating also the change in nanowire diameter across the heterojunction. The average diameters are 35 nm for the InAs part and 50 nm for the GaSb part, measured by transmission electron microscopy.[15] The composition of the nanowire does not shift abruptly between InAs and GaSb, instead a gradual change over 30−50 nm occurs.[15] Investigations by X-ray photoemission spectroscopy (XPS) and X-ray photoemission electron microscopy (XPEEM) have additionally found that the nanowire surface region on both the GaSb and InAs parts consists of a ∼1 nm thick layer that contains oxides of all four elements (Ga, Sb, In, and As).[16] Such a surface layer is especially significant for this work due to the high surface sensitivity of the STM/STS measurements.

Device fabrication was performed on n++ doped Si/SiO_2 substrates (200 nm SiO_2) with details described in ref 15. In brief, nanowires were deposited onto device substrates with prefabricated 80 nm thick Ti/Au electrical contacts, patterned by mask aligned UV photolithography and markers for nanowire locating patterned by electron beam lithography (EBL). Prior to deposition, the nanowires were exposed to oxygen plasma (at 5 mTorr O_2 pressure) for 45 s and placed in 1:9 HCl/H_2O solution for 30 s in order to remove any residual resist and to reduce the native oxide thickness.

Prior to AFM/STM measurements the nanowire devices had to be cleaned from their native oxide and possible adsorbates. Several procedures for oxide removal from nanowires have been suggested in literature, including chemical etching and passivation,[17,18] As capping and later on evaporation for nanowires grown by molecular beam epitaxy[10,19] and annealing in the presence of atomic hydrogen.[8,20] Various approaches and experimental conditions are discussed in the Supporting Information. We obtained best results by cleaning the nanowire devices in vacuum using atomic hydrogen (provided by a thermal cracker) at a pressure of 2 × 10^{-6} mbar for 30 min at 380 °C. Annealing to higher temperatures was not possible as

DOI: 10.1021/acs.nanolett.5b00898
Nano Lett. 2015, 15, 3684−3691

the design of the nanowire device structure cannot withstand temperatures above 400 °C. However, while this procedure is sufficient to achieve structurally ordered oxygen free surfaces on InAs or InP,[9,11] the temperatures are not high enough to fully remove Ga oxides or mixed oxides found in the present case. XPEEM and XPS measurements confirm a significant thinning of the oxide layer upon hydrogen cleaning.[16] However, it is important to note that even after cleaning very thin surface layers with traces of Ga, In, As, Sb, and O are found to be present at both nanowire segments. Nevertheless, stable conditions for STM/STS on top of the InAs–GaSb Esaki diode nanowires were achieved upon cleaning.

The cleaned nanowire devices were investigated at room temperature in an Omicron VT dual AFM/STM at 10^{-11} mbar ultrahigh vacuum (UHV) using Omicron qPlus sensors with an all-metallic tungsten combined AFM/STM tip. The tungsten tips were prepared in UHV by Ar-ion sputtering. The AFM/STM has four external electrical contacts which were used to apply a bias, V_{NW}, to the contact electrodes on the device sample inside the AFM/STM. Figure 1b shows a schematic representation of a device inside the AFM/STM with the tip and the external biasing of the nanowire.

For the initial positioning of the tip, we used an optical camera attached to the AFM/STM together with markers that were created on the sample during nanowire device fabrication. In order to locate the nanowire device of interest, the AFM mode was used in low resolution, typically recording approximately 10 μm^2 images, Figure 1c. Once found, higher resolution AFM images, Figure 1d, were used to precisely explore the nanowire and its topographic features. When the nanowire was located, the AFM/STM tip was positioned on top of the nanowire. By switching to STM mode, nanoscale resolution imaging of the nanowire surface and the possibility to conduct STS measurements was enabled. For STS point spectra, the tip was placed at an area of interest and the total conductance $I-V$ and the differential conductance $(dI/dV) - V$ were measured simultaneously. For the $(dI/dV) - V$ measurements, a lock-in amplifier was used with an alternating current amplitude of V_{mod} = 80 mV and a modulation frequency of f_{mod} = 1.1 kHz. To increase the dynamic range of the STS measurements at the band edges, a variable gap mode was used where the tip–sample separation was decreased with decreasing absolute value of the bias by 2 Å/V.[9,21] The $(dI/dV) - V$ spectra were normalized to the total conductance that was broadened by convolution with an exponential function, as described in ref 21, using a broadening width of 0.2 V. For this particular experiment it is also relevant to point out that for the Omicron AFM/STM used here the tip–sample tunnel bias (V_T) during STM and STS experiments is applied to the tip (relative to ground) and not to the sample. This tunnel bias has to be distinguished from the bias applied between different contacts of the sample (V_{NW}, also relative to ground). Because of our experimental setup we have therefore chosen to show the tunneling current as a function of tip potential (instead of sample potential which is more common for STM experiments) to facilitate the interpretation of the STS data.

Figure 2 illustrates the various possibilities of our setup for quantitatively analyzing the nanowire surface electronic properties, morphology, and the device response to an applied bias. Importantly, during all stages of the experiment the Esaki diode behavior of the nanowire under study and thus the integrity of the device could be verified by measuring the conductance

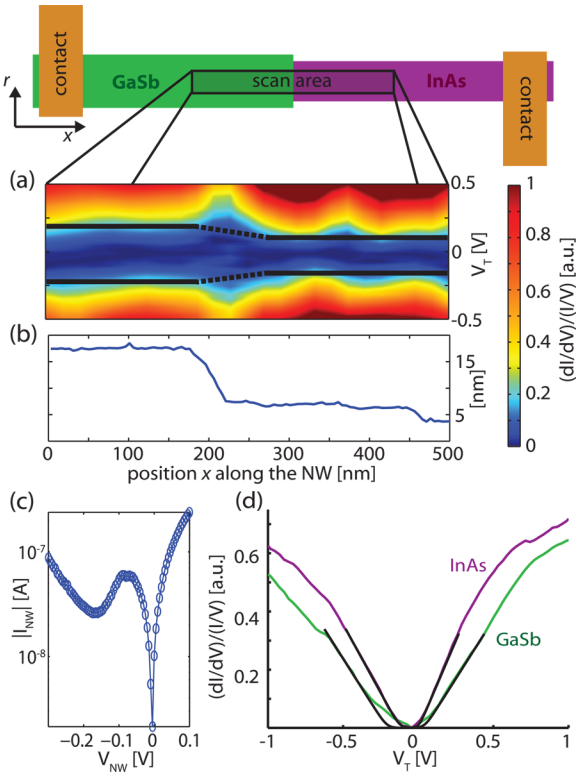

Figure 2. (a) $(dI/dV) - V$ spectra, recorded along the grounded nanowire, are shown in a contour plot, revealing the change in bandgap across the GaSb–InAs interface with a transition area between x = 180 and 240 nm. From evaluating the band onsets in the individual spectra, a bandgap of 0.39 ± 0.03 eV at the surface of the GaSb part and 0.20 ± 0.05 eV at the surface of the InAs part was obtained, as shown by Figure S5 of the Supporting Information. These bandgaps are indicated by black lines. (b) Height profile of the 500 nm long area across the InAs–GaSb interface where the spectra in (a) were recorded. Here the change in diameter between the thicker GaSb and the thinner InAs part of the nanowire is clearly seen, extending between x = 180 and 220 nm. (c) A typical conductance measurement of the Esaki diode showing the absolute current through the nanowire, I_{NW}, as a function of the applied bias, V_{NW}, (with the GaSb part of the nanowire grounded and the bias potential applied to the InAs part) as measured inside the STM with the external contacts. (d) STS spectra were averaged separately for the surfaces of the InAs (magenta) and of the GaSb part (green) of the Esaki diode nanowire with both external contacts to the nanowire grounded, V_{NW} = 0, showing the normalized differential conductance, $(dI/dV)/(I/V)$, as a function of the tip potential, V_T. The fitted functions used to derive the valence (VB) and conduction band (CB) onsets are also shown as black lines (see Supporting Information for more details).

through the nanowire, as seen in Figure 2c. Such a behavior corresponds to a broken band alignment.[12,13,15]

First, standard STM images along the nanowire were recorded. A height profile from such an image is shown in Figure 2b with a lateral resolution of <1 nm. The 10 nm large step indicates the transition from GaSb to InAs, which is consistent with the (on average) 25 to 17 nm radius change of the nanowire described above.

In order to study the local electronic structure along the surface of the nanowire device, we performed STS across the GaSb–InAs heterojunction. In Figure 2a, we show 25 spectra of the normalized differential conductance, equidistantly placed with 20 nm separations along the nanowire surface across the GaSb–InAs interface. When the tip moves from the GaSb part

DOI: 10.1021/acs.nanolett.5b00898
Nano Lett. 2015, 15, 3684–3691

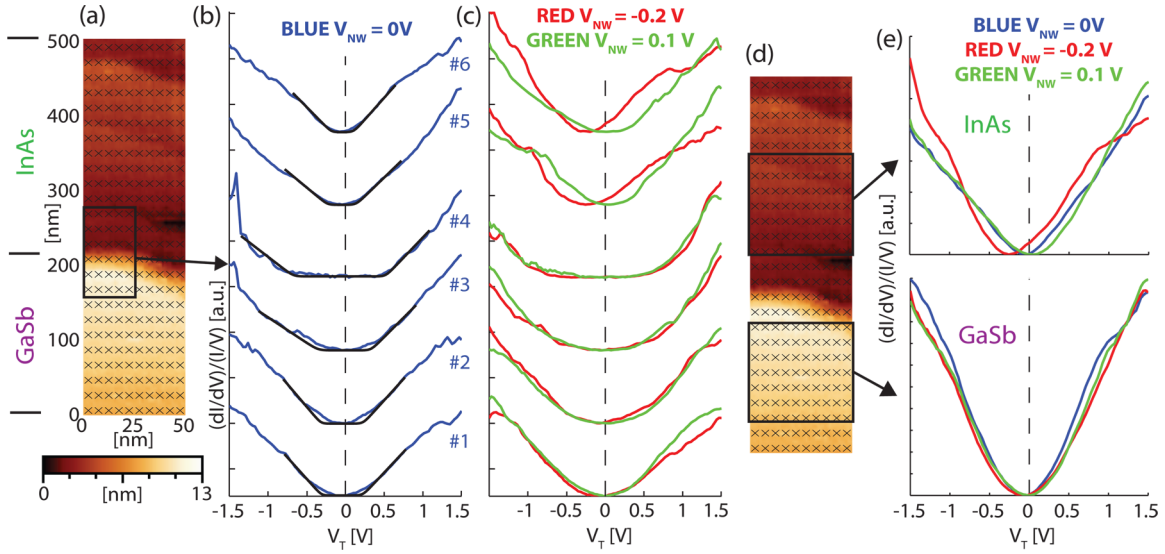

Figure 3. (a) STM image of the nanowire showing the thicker GaSb part (bottom) and the thinner InAs part (top). A 10 × 25 grid defining the positions of the STS spectra is shown overlaid (x). (b) STS spectra from the surface at the InAs−GaSb transition area are plotted, as indicated by the black rectangle in (a), averaged over five adjacent spectra each. The change from GaSb- to InAs-like properties is shown to occur between three spectra (number 3 to 5), that is, over 40 nm. The spectra in the center of this transition region show significant broadening of the bandgap. Fitted CB and VB onsets are indicated by black lines. Spectra shown in (b) were recorded with the nanowire grounded, V_{NW} = 0 V, while spectra shown in (c) were recorded while a bias of V_{NW} = 0.1 V (green) and V_{NW} = −0.2 V (red) was applied to the nanowire. (e) The average of 70 spectra recorded on the surface at the InAs (top) and GaSb (bottom) part of the nanowire is plotted with their position indicated by the black rectangles in (d). Blue spectra are recorded at V_{NW} = 0 V, red at V_{NW} = −0.2 V, and green at V_{NW} = 0.1 V. The spectra obtained at the GaSb part show consistent behavior independent of V_{NW}. However, for the spectra at the InAs part the position of the bandgap shifts when a bias is applied corresponding to the change in V_{NW}.

to the InAs part, a change from a wider to a smaller bandgap material is observed with the transition occurring in the region from x = 180−240 nm. Averaged STS spectra from the surface at the InAs part (magenta) and the surface at the GaSb part (green) of the nanowire are shown in Figure 2d. The normalized differential conductance $(dI/dV)/(I/V)$, which is plotted here, has been shown to represent the local density of states (LDOS) at the surface.[22,23] In the spectra of Figure 2d, a small but distinct region of low density of states can be found around 0 V, enclosed by a homogeneous and almost linear increase of the LDOS at larger absolute bias. This increase of the LDOS can well be fitted with a linear expression convoluted with small thermal broadening, as shown by the black curves in Figure 2d, and we therefore consider it as the valence and conduction band onset, in accordance to the method described in ref 21 (assuming a linear increase of the LDOS near the band edges). Thus, these fitted band edges define a band gap E_g. Average bandgaps of the nanowire surface at the InAs and the GaSb part were determined to be 0.20 ± 0.05 and 0.39 ± 0.03 eV, respectively, as obtained from 250 STS spectra which were recorded in a 50 × 500 nm^2 area over the GaSb−InAs junction (see Supporting Information for more details). At both parts, the bandgaps are centered at −0.05 ± 0.02 V.

The experimentally observed surface bandgaps are smaller than the bulk values for InAs and GaSb bandgaps of 0.35 and 0.73 eV (at room temperature). Even more remarkably, the observed surface bandgaps (with the nanowire grounded) at both parts of the nanowire are centered close to 0 V, although the InAs part of the nanowire is n-type and the GaSb part p-type. Before we discuss possible explanations for this behavior, we want to summarize the experimental facts: In STS spectra, the Fermi level is always located at 0 V, independent of sample doping or surface states.[23,24] All our observed spectra show a clear rise of the conductivity at both negative and positive voltages with a well-defined region of low conductivity in between, which is centered close to the Fermi level. This observation is valid for $I-V$ spectra and for simultaneously obtained $dI/dV - V$ spectra, as well as for spectra of the normalized differential conductance $(dI/dV)/(I/V)$ using various broadening, as shown in detail in the Supporting Information, Figure S3. Thus, the rather small apparent band gaps at both segments of the nanowire, and their relative energy position with the Fermi level close to midgap, are inherent properties of our nanowire surface and are not due to data processing or interpretation.

The remaining question that needs to be discussed is the origin of these surface electronic properties. These are especially remarkable because at the same time we observe Esaki diode behavior of the nanowire (Figure 2c), which requires a broken bandgap configuration between n-doped InAs and p-doped GaSb at the core of the nanowire. In the following, we will discuss three possible contributions to this discrepancy, that is, surface states, tip-induced band bending, and a thin shell layer of different composition at the nanowire surface. These three contributions are all based on the strong surface sensitivity of the STM results. Generally, the presence of dopants[21] or surface states[25] is known to result in an increased LDOS within the bulk semiconductor bandgap, which can be seen in $dI/dV - V$ spectra. While nonpolar nanowire surfaces (as those studied here) generally have no surface states when they are oxide and defect free,[8,26] previous measurements also indicate that the presence of oxides can induce interface states.[9,27] However, surface states or dopants typically only give a small dI/dV signal, which is much weaker than the contribution from the conduction or valence band. However, the spectra observed here show a monotonic increase of the

DOI: 10.1021/acs.nanolett.5b00898
Nano Lett. 2015, 15, 3684−3691

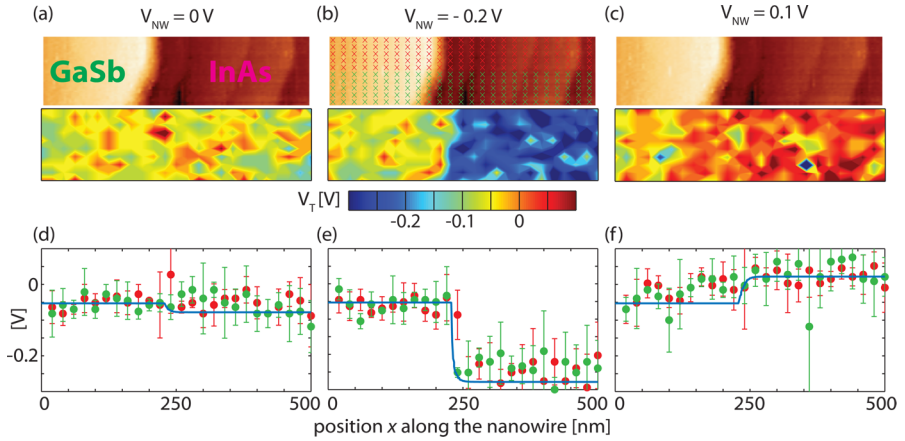

Figure 4. (a–c) Three STM images and the corresponding contour maps (10 × 25 STS spectra each) showing the position of the middle of the bandgap for each spectrum recorded with V_{NW} = 0, −0.2, and 0.1 V (the bias applied to the contact connected to the InAs part (right) of the nanowire). The STM image (b) recorded simultaneously with the STS spectra at V_{NW} = −0.2 V shows that the change in surface bandgap position is aligned with the height change between the GaSb and the InAs part of the nanowire. The positions of the STS spectra are indicated (x). (d–f) The mean value of the bandgap energy position in each column of spectra is shown with respect to position x along the nanowire in order to illustrate the change in surface potential along the nanowire for V_{NW} = 0, −0.2, and 0.1 V, respectively. Red dots correspond to the upper half of the nanowire and green to the lower, as indicated in (b), and error bars show the standard deviation of the mean. The blue line is the potential through the core of the nanowire as calculated using COMSOL Multiphysics. The line is calibrated with the small ground offset (−0.053 V) from the measured data.

LDOS at both sides of the bandgap, as one should expect for the conduction band and valence band, with no additional confined states. We cannot exclude the existence of surface states that strongly overlap with the onset of the conduction or valence band but at least we cannot distinguish such states. Tip-induced band bending as an effect of the electric field between the sample and the STM tip is known to shift the energy position of the bands at the sample surface in STS experiments, leading to wrong numbers of the absolute band gap.[8,28,29] However, such tip-induced band bending generally increases the apparent bandgap as measured with STS, while the surface bandgaps observed here are smaller than expected. As mentioned above, we know from XPS and XPEEM measurements that even after cleaning the nanowire devices there still is a very thin surface layer, containing a mixture of Ga, In, As, Sb, and probably O, covering the entire nanowire. Therefore, we actually should not expect to find a bulk InAs-like n-type bandgap at the surface of the InAs part or a bulk GaSb-like p-type bandgap at the surface of the GaSb part of the nanowire. Instead, the LDOS at the nanowire surface probably results from an interplay of the band alignment of the InAs and GaSb core parts with the thin surface layer. It has been shown that a few monolayer thin metallic film on GaAs can result in $dI/dV - V$ spectra showing a still well-defined bandgap but of decreased width, as compared to bulk GaAs,[30] a similar effect as we observe here. We cannot finally say if the surface layer has a different chemical composition at the InAs and GaSb parts of the nanowire, resulting in surface bandgaps of different width, or if a similar surface layer interacting with either the InAs or the GaSb core leads to differently resulting surface bandgaps.

Importantly, the significantly different electronic situation at the nanowire surface does not impede the Esaki diode performance of the nanowire, which has to be enabled by the band alignment at the nanowire core. In a simplified picture, we can describe the different situations between nanowire core and surface by a surface Fermi-level being pinned midgap, extending radially into the nanowire by band bending: The extension of the band bending can be calculated as described by ref 27, where the cylindrical geometry of the NW is taken into consideration, to 7 nm for the GaSb part (with a p-doping of 1 × 10^{19} cm^{-3}) and 16 nm for the InAs part (with an n-doping of 1 × 10^{18} cm^{-3}), resulting in a sufficiently wide core region of the nanowire not being, or only weakly, affected by the surface level pinning (see Supporting Information). Even if we cannot definitely determine the origin of the observed small surface bandgaps, we can though conclude that our experimental setup can simultaneously reveal the band alignment both in the core of the nanowire, as obtained from the device conductance behavior, and locally along the nanowire surface as shown by the STS spectra.

While scanning a 50 × 500 nm^2 area across the InAs–GaSb interface 250 STS spectra were recorded in a 10 × 25 matrix spaced over the whole image. Figure 3a shows an STM image of the interface with the thicker GaSb part at the bottom of the image and the InAs part at the top with the positions where the spectra were taken marked with x. Zooming in on the transition region between the GaSb and InAs, we plot average $(dI/dV)/(I/V) - V$ spectra, Figure 3b, from the transition region where each spectra is the result of averaging five measurements at the same specific position x along the nanowire. The left side of the nanowire, Figure 3a, is used for the averaging due to the slight inhomogeneity of the transition region on the right side of the nanowire as seen in the STM image. Generally a good reproducibility of the spectra taken at the same nanowire material can be observed. Minor fluctuations from spectra to spectra along the nanowire can be attributed both to some remaining instability of the STS measurements especially at higher voltages but also to local variations in the composition and thickness of the surface layer. The transition from more GaSb- to more InAs-like STS spectra is found to occur over three subsequent spectra, that is, over 40 nm, coinciding with the change in nanowire diameter, Figure 3a.

Interestingly, right at the transition between both parts of the nanowire a significant widening of the apparent bandgap is observed; the measured bandgap is larger than what is observed at the surface at both the GaSb and InAs parts. This widening is consistently observed in the measurements (even if a bias is applied to the nanowire, as will be discussed below) and

DOI: 10.1021/acs.nanolett.5b00898
Nano Lett. 2015, 15, 3684–3691

appears to influence spectra in a 20−40 nm wide region (1−2 rows) around the diode junction. As mentioned above, the interface between the GaSb and InAs parts of the nanowire is not fully abrupt but consists of an about 20−30 nm wide transition region of graded InGaAsSb composition.[15] This transition region can be expected to be electronically depleted, acting as an additional tunnel barrier. Broadening of the surface bandgap in the depletion region has been observed previously for the depletion region of GaAs pn-junctions using cross-sectional STM.[24,31] While the surface in that case was clean GaAs(110) we note that even in the present case of a multielement surface layer along the nanowire, the depletion region inside the wire causes a broadening of the surface bandgap in the transition region of the wire. This broadening might be further enhanced by a stronger effect of tip-induced band bending at the depletion region. We postulate that this bandgap broadening could help explain the excellent functionality of these nanowire Esaki diodes, because without it the surface of the nanowire, showing small bandgaps and no broken-gap alignment, would electronically short the nanowire device.

Next, we study how the nanowire is affected as different bias voltages are applied to the contact to the InAs part of the nanowire. The resulting changes in the STS spectra along the nanowire can be seen in Figure 3c for $V_{NW} = -0.2$ V (red) and $V_{NW} = 0.1$ V (green). Figure 3e shows STS results where 70 spectra were averaged over a larger area to take out the influence of local fluctuations in the surface composition along the nanowire. The spectra obtained at the surface of the GaSb part of the nanowire are found to be hardly influenced by the bias V_{NW}, which is applied to the InAs contact. At the surface of the InAs part, however, a clear shift in the onset of the $(dI/dV)/(I/V)$ signal is observed especially for the spectra recorded at $V_{NW} = -0.2$ V, which turns out to reflect the potential along the nanowire device as compared to the unbiased case.

The onset of the $(dI/dV)/(I/V)$ signal corresponds to the edges of the valence and conduction band. In order to further investigate how the local energy positions of the band edges along the nanowire surface shift as a response to the applied bias, we evaluate the center energy position of the bandgap region relative to $V_T = 0$ V for every spectrum (see Supporting Information for more details). These values are then plotted as a function of the position over the nanowire in Figure 4a−c. Thus, the contour plots of Figure 4a−c show how the energy position of the bandgap and hence how the local potential along the surface of the nanowire is changed when a bias is applied to the nanowire device. In order to further illustrate this, one could consider the example of performing STS on a metallic surface. In the standard situation the metal is grounded, it has no bandgap region, and a current onset will be found at $V_T = 0$ V. If the potential of the metal is changed to −0.2 V the current onset will be at $V_T = -0.2$ V, analog with the shift in bandgap energy position (for different potentials) seen in our measurements.

In the case of a grounded nanowire, $V_{NW} = 0$ V, the bandgap position is constant along the entire nanowire with only small random fluctuations, Figure 4a. This is consistent with the Fermi level being close to midgap of the small surface bandgaps found at both parts of the nanowire. The width of the surface bandgap changes, as mentioned earlier, from 0.39 to 0.20 eV going from the GaSb to the InAs part, but the center of the bandgap remains constant at an average value of −0.05 eV along the nanowire for $V_{NW} = 0$ V.

When a potential of $V_{NW} = -0.2$ V is applied to the InAs contact of the nanowire, Figure 4b, the contour plot shows two distinct regions of different surface potential. By comparing this contour plot with the simultaneously recorded STM image of the nanowire, it becomes clear that a significant potential drop is seen over the GaSb−InAs interface with a negative surface potential at the InAs part. When a positive potential of $V_{NW} = 0.1$ V is applied, Figure 4c, the InAs part of the nanowire shows a positive surface potential, but the transition toward the GaSb part is less distinct than for the case of a negative potential. This behavior can qualitatively be explained by the Esaki diode behavior of the GaSb−InAs heterojunction: A potential of $V_{NW} = -0.2$ V applied to the InAs contact corresponds to the conductance valley of the Esaki diode, Figure 2c, and hence the potential drops almost completely at the interface. A potential of $V_{NW} = 0.1$ V, however, corresponds to a much higher conductivity across the Esaki diode, Figure 2c, and in this case the Ohmic resistance of the GaSb part of the nanowire contributes significantly to the entire device resistance,[13] so that a significant part of the applied bias drops over the GaSb part. The potential drop in the nanowire core is reflected by the smooth transition of the surface potential along the GaSb part of the nanowire, as seen in Figure 4c. This result is even more remarkable, because the band alignment at the surface is strongly different from that in the nanowire core, as discussed above. It is consistent with a picture in which the local potential inside the nanowire determines the ground level of the STM measurement at a specific position along the nanowire. Thus, our STS measurements give a measure of the local potential distribution inside the nanowire, alongside probing the separate surface bandstructure.

To clarify the change in surface potential not only along but also perpendicular to the nanowire growth axis, we divide the spectra into two halves, one upper (red x) and one lower (green x) half, Figure 4b. Next, we obtain the mean value of the bandgap energy position for those spectra that are obtained at the same position x along the nanowire, separately for the upper and lower half (green and red columns of spectra in Figure 4b). In Figure 4d−f, we plot these mean values over the position x for both halves with error bars (showing the standard deviation of the mean). Generally the values obtained from both halves of the nanowire correspond very well, indicating that the wire is homogeneous perpendicular to its growth axis. However, at the interface between the GaSb and InAs parts (where the change in surface potential occurs) a difference between the two halves of the nanowire is observed for an applied bias of $V_{NW} = -0.2$ V, Figure 4e; the potential change occurs 20 nm further to the left on the lower half. This corresponds well to the different position of the transition from GaSb to InAs nanowire diameter when comparing the upper and lower halves of the nanowire in the corresponding STM image seen in Figure 4a−c. The correlation between the surface potential and structural changes over the nanowire indicates that we can relate morphology and local electronic structure.

In order to also quantitatively explain the shifts of the bandgap energy position measured along the nanowire upon applied bias, we have performed COMSOL Multiphysics simulations of the potential in the core of the nanowire along the axial direction (see Supporting Information). The results are plotted in Figure 4d−f as a blue line along with the measured bandgap energy position. For $V_{NW} = -0.2$ V, the calculated potential in the nanowire core changes from −0.2 to 0 V in a small region of <20 nm at the InAs−GaSb interface,

DOI: 10.1021/acs.nanolett.5b00898
Nano Lett. 2015, 15, 3684−3691

which is consistent with the abrupt change observed experimentally for the surface potential. It should be noted though that the local surface potential appears to be fluctuating with 0.05 V along the biased InAs part, which could be due to small changes in the actual pinning position along the nanowire as the local composition of the surface oxide could differ. For V_{NW} = 0.1 V the simulations show an abrupt change of the potential in the nanowire core at the heterojunction. The experimentally obtained surface potential at the InAs part is constant at 0.1 V, whereas at the GaSb part it slowly drops toward the grounded value while moving away from the interface. This inconsistency can however be explained by the Ohmic resistance of the GaSb part discussed above, which is not taken into account in the simulation.

In conclusion, we demonstrate the first example of STM and STS measurements on an individually contacted nanowire during device operation. Using the external electrical contacts the Esaki diode behavior, and thereby the broken band alignment of the InAs−GaSb nanowire, could be confirmed during all stages of the experiment. This is in strong contrast to the band alignment at the nanowire surface, which shows small bandgaps with the Fermi level close to midgap, probably due to a thin intermixed surface layer along the entire nanowire. Surface band gaps were obtained from STS measurements for the GaSb part with 0.39 ± 0.03 eV and for the InAs part with 0.20 ± 0.05 eV. Even more, the electronic structure at the surface is influenced by the Esaki diode transition region found inside, effectively creating a broad gap with an extension of 20 to 40 nm around the diode interface in the otherwise rather conductive surface. It was further found that a potential drop in the nanowire, created by an applied bias, is directly reflected by local changes of the nanowire surface potential, which can be monitored by STM/S. Thus, we have presented a method that can exactly probe the band alignment inside and along the surface of a nanowire at the same time.

This experiment has proven that STM/S investigations of complicated III−V nanowires in a device configuration are possible even during device operation. The ground level of the surface sensitive STM measurement will be determined by the local potential inside the biased nanowire. We have shown how to gain information on the surface local density of states of a real device, including the surface band alignment across the interface, and how these properties change upon device operation. These results clear the way for a novel approach to nanostructure device characterization, where not only the influence of device operation on its surface and contact properties is explored, but where also the direct interplay between nanometer-scale surface properties and device performance is revealed and utilized for tailoring future devices.

■ ASSOCIATED CONTENT

Supporting Information

Surface potential mapping, evaluation of dI/dV−V spectra and bandgaps, calculations of surface band bending, the COMSOL Multiphysics simulation, nanowire surface cleaning, and Figures S1−S5. The Supporting Information is available free of charge on the ACS Publications website at DOI: 10.1021/acs.nanolett.5b00898.

■ AUTHOR INFORMATION

Corresponding Author

*E-mail: rainer.timm@sljus.lu.se.

Notes

The authors declare no competing financial interest.

■ ACKNOWLEDGMENTS

This work was performed within the Nanometer Structure Consortium at Lund University, and was supported by the Swedish Research Council (VR), the Swedish Foundation for Strategic Research (SSF), the Crafoord Foundation, the Knut and Alice Wallenberg Foundation, and the European Research Council under the European Union's Seventh Framework Programme, Grant Agreement No. 259141. One of the authors (R.T.) acknowledges support from the European Commission under the Marie Curie Intra-European Fellowship "NanowireDeviceSTM".

■ REFERENCES

(1) Minot, E. D.; Kelkensberg, F.; van Kouwen, M.; van Dam, J. A.; Kouwenhoven, L. P.; Zwiller, V.; Borgström, M. T.; Wunnicke, O.; Verheijen, M. A.; Bakkers, E. P. A. M. *Nano Lett.* **2007**, *7* (2), 367−371.

(2) Wallentin, J.; Anttu, N.; Asoli, D.; Huffman, M.; Åberg, I.; Magnusson, M. H.; Siefer, G.; Fuss-Kailuweit, P.; Dimroth, F.; Witzigmann, B.; Xu, H. Q.; Samuelson, L.; Deppert, K.; Borgström, M. T. *Science* **2013**, *339* (6123), 1057−1060.

(3) Tian, B.; Zheng, X.; Kempa, T. J.; Fang, Y.; Yu, N.; Yu, G.; Huang, J.; Lieber, C. M. *Nature* **2007**, *449* (7164), 885−889.

(4) Duan, X.; Huang, Y.; Cui, Y.; Wang, J.; Lieber, C. M. *Nature* **2001**, *409* (6816), 66−69.

(5) Zhang, S.; Hemesath, E. R.; Perea, D. E.; Wijaya, E.; Lensch-Falk, J. L.; Lauhon, L. J. *Nano Lett.* **2009**, *9* (9), 3268−3274.

(6) van Weert, M. H. M.; Wunnicke, O.; Roest, A. L.; Eijkemans, T. J.; Yu Silov, A.; Haverkort, J. E. M.; 't Hooft, G. W.; Bakkers, E. P. A. M. *Appl. Phys. Lett.* **2006**, *88* (4), 043109.

(7) Wernersson, L. E.; Thelander, C.; Lind, E.; Samuelson, L. *Proc. IEEE* **2010**, *98* (12), 2047−2060.

(8) Hjort, M.; Lehmann, S.; Knutsson, J.; Timm, R.; Jacobsson, D.; Lundgren, E.; Dick, K. A.; Mikkelsen, A. *Nano Lett.* **2013**, *13* (9), 4492−4498.

(9) Hjort, M.; Wallentin, J.; Timm, R.; Zakharov, A. A.; Håkanson, U.; Andersen, J. N.; Lundgren, E.; Samuelson, L.; Borgström, M. T.; Mikkelsen, A. *ACS Nano* **2012**, *6* (11), 9679−9689.

(10) Capiod, P.; Xu, T.; Nys, J. P.; Berthe, M.; Patriarche, G.; Lymperakis, L.; Neugebauer, J.; Caroff, P.; Dunin-Borkowski, R. E.; Ebert, P.; Grandidier, B. *Appl. Phys. Lett.* **2013**, *103* (12), 122104.

(11) Hjort, M.; Lehmann, S.; Knutsson, J.; Zakharov, A. A.; Du, Y. A.; Sakong, S.; Timm, R.; Nylund, G.; Lundgren, E.; Kratzer, P.; Dick, K. A.; Mikkelsen, A. *ACS Nano* **2014**, *8* (12), 12346.

(12) Borg, B. M.; Dick, K. A.; Ganjipour, B.; Pistol, M.-E.; Wernersson, L.-E.; Thelander, C. *Nano Lett.* **2010**, *10* (10), 4080−4085.

(13) Ganjipour, B.; Dey, A. W.; Borg, B. M.; Ek, M.; Pistol, M.-E.; Dick, K. A.; Wernersson, L.-E.; Thelander, C. *Nano Lett.* **2011**, *11* (10), 4222−4226.

(14) Ek, M.; Borg, B. M.; Johansson, J.; Dick, K. A. *ACS Nano* **2013**, *7* (4), 3668−3675.

(15) Webb, J.; Persson, O.; Dick, K.; Thelander, C.; Timm, R.; Mikkelsen, A. *Nano Res.* **2014**, *7* (6), 877−887.

(16) Mårsell, E. Manuscript in preparation.

(17) Suyatin, D. B.; Thelander, C.; Björk, M. T.; Maximov, I.; Samuelson, L. *Nanotechnology* **2007**, *18* (10), 105307.

(18) Cui, Y.; Wang, J.; Plissard, S. R.; Cavalli, A.; Vu, T. T. T.; van Veldhoven, R. P. J.; Gao, L.; Trainor, M.; Verheijen, M. A.; Haverkort, J. E. M.; Bakkers, E. P. A. M. *Nano Lett.* **2013**, *13* (9), 4113−4117.

(19) Tao, X.; Kimberly, A. D.; Sébastien, P.; Thanh Hai, N.; Younes, M.; Maxime, B.; Jean-Philippe, N.; Xavier, W.; Bruno, G.; Philippe, C. *Nanotechnology* **2012**, *23* (9), 095702.

DOI: 10.1021/acs.nanolett.5b00898
Nano Lett. 2015, 15, 3684−3691

(20) Hilner, E.; Håkanson, U.; Fröberg, L. E.; Karlsson, M.; Kratzer, P.; Lundgren, E.; Samuelson, L.; Mikkelsen, A. *Nano Lett.* **2008**, *8* (11), 3978−3982.
(21) Feenstra, R. M. *Phys. Rev. B* **1994**, *50* (7), 4561−4570.
(22) Lang, N. D. *Phys. Rev. B* **1986**, *34* (8), 5947−5950.
(23) Stroscio, J. A.; Feenstra, R. M.; Fein, A. P. *Phys. Rev. Lett.* **1986**, *57* (20), 2579−2582.
(24) Feenstra, R. M.; Yu, E. T.; Woodall, J. M.; Kirchner, P. D.; Lin, C. L.; Pettit, G. D. *Appl. Phys. Lett.* **1992**, *61* (7), 795−797.
(25) Feenstra, R. M.; Lee, J. Y.; Kang, M. H.; Meyer, G.; Rieder, K. H. *Phys. Rev. B* **2006**, *73* (3), 035310.
(26) Hilner, E.; Lundgren, E.; Mikkelsen, A. *Surf. Sci.* **2010**, *604* (3−4), 354−360.
(27) Wang, D.; Chang, Y.-L.; Wang, Q.; Cao, J.; Farmer, D. B.; Gordon, R. G.; Dai, H. *J. Am. Chem. Soc.* **2004**, *126* (37), 11602−11611.
(28) Feenstra, R. M.; Stroscio, J. A.; Fein, A. P. *Surf. Sci.* **1987**, *181* (1−2), 295−306.
(29) Timm, R.; Feenstra, R. M.; Eisele, H.; Lenz, A.; Ivanova, L.; Lenz, E.; Dähne, M. *J. Appl. Phys.* **2009**, *105* (9), 093718.
(30) Shih, C. K.; Feenstra, R. M.; Mårtensson, P. *J. Vac. Sci. Technol. A* **1990**, *8* (4), 3379−3385.
(31) Jäger, N. D.; Marso, M.; Salmeron, M.; Weber, E. R.; Urban, K.; Ebert, P. *Phys. Rev. B* **2003**, *67* (16), 165307.

DOI: 10.1021/acs.nanolett.5b00898
Nano Lett. 2015, 15, 3684−3691